Structure of Interfaces in Cu|Au Nanolaminates

A. Gola, L. Pastewka

published in

NIC Symposium 2018
K. Binder, M. Müller, A. Trautmann (Editors)

Forschungszentrum Jülich GmbH,
John von Neumann Institute for Computing (NIC),
Schriften des Forschungszentrums Jülich, NIC Series, Vol. 49,
ISBN 978-3-95806-285-6, pp. 247.
http://hdl.handle.net/2128/17544

Structure of Interfaces in Cu|Au Nanolaminates

Adrien Gola and Lars Pastewka

Institute for Applied Materials, Karlsruhe Institute of Technology,
Straße am Forum 4, 76131 Karlsruhe, Germany

Department of Microsystems Engineering, University of Freiburg,
Georges-Köhler-Allee 103, 79110 Freiburg, Germany
E-mail: lars.pastewka@imtek.uni-freiburg.de

We used molecular dynamics calculations to study the influence of interdiffusion on the bicrystal interface of Cu|Au nanolaminates. Starting from an ideal bicrystal of 50 nm thickness with a $\{111\}$ semi-coherent interface, we created a diffusive interface region and annealed the system at 1000 K. We report the resulting interfacial crystallographic defects as a function of interface width. Our results show an increase of dislocation spacing as the interface becomes more diffuse. The most diffuse interfaces of $\sim$ 10 nm width studied here form stacking fault tetrahedra.

1 Introduction

Crystalline metallic nanolaminates, often also called multilayers or heterostructures, are material systems that consist of layers of alternating stoichiometry. The interfaces between layers play an important role in their mechanical properties, because they can act as barriers, sinks or sources for dislocations[1–5].

The structure of a heterointerface adjusts to accommodate the misfit in lattice constant and elastic modulus from one layer to the next. Structure therefore depends on lattice parameters, which can for example be controlled by alloying, and it is decisive for the control of mechanical properties of these materials. Nanolaminates are therefore potential candidates for future engineering materials with tailored mechanical properties, but they are also useful as a laboratory for the study of dislocations interacting with interfaces[6], the influence of microstructure on mechanical properties[5–7] or alloying by mechanical action[8,9].

A prototypical nanolaminate is the Cu-Au system. Phase separated films of Cu-Au have been prepared experimentally for decades[10–12]. Cu and Au both crystallise in the face-centred cubic (FCC) structure. They are miscible and form stable intermetallic phases. The phase separated state is therefore an example of a material far from equilibrium.

For non-miscible metals such as Cu and Ni, the heterointerface is often semi-coherent, consisting of a network of Shockley partial dislocations separated by stacking faults[13,14]. The structure for heterointerfaces of miscible compounds such as Cu|Au is less clear because of the tendency of the interface to diffusively intermix. The concentration then varies continuously from one side to the other. We here report on a study of the structure of dislocation networks at these interfaces as a function of the width of this intermixed layer using atomistic simulation methods.

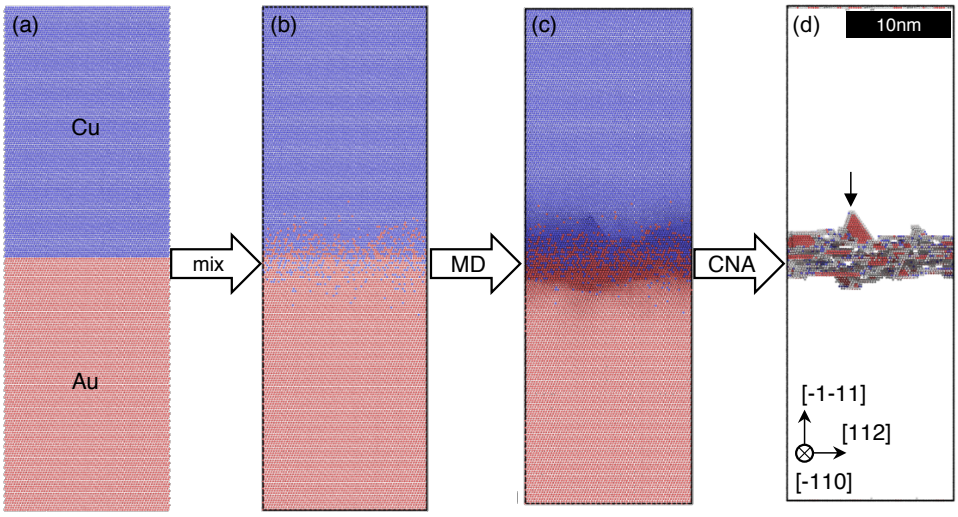

Figure 1. Illustration of the simulation procedure. We start with (a) an initial perfect Cu|Au system composed of two single crystals and then (b) intermix the interface region by randomly swapping atoms to achieve the concentration profile given by Eq. 2. (c) This system then annealed and aged. (d) We then use a common neighbour analysis (CNA) to identify atoms not in their ideal face-centred cubic (FCC) environment. Atoms are coloured according to their chemical element in figures (a-c) with Cu in blue and Au in red. Atoms in (d) are coloured according to their local lattice structure with hexagonal close packed (HCP) atoms in red, body-centred cubic (BCC) atoms in blue and structures unidentified by the CNA in white.

2 Methods

2.1 Atomic-Scale Interface Model

We used atomistic simulations to study the interface between Cu and Au in these nanolaminates. Our initial system was composed of two perfect crystals of Cu and Au stacked along the $[\bar{1}\bar{1}1]$ directions (Fig. 1a). The height of each crystal was ~ 25 nm. The two other axes of the orthorhombic simulation cell were oriented along the $[112]$ and the $[\bar{1}10]$ directions for both crystals. The simulation box was periodic along the $[112]$ and $[\bar{1}10]$ directions, with a free boundary in the $[\bar{1}\bar{1}1]$ direction.

In order to minimise the stresses arising from the large lattice misfit ($\delta \approx 12\%$) between the Cu and Au crystals, the lateral cell size needed to be commensurate with the lattice constant of both Cu and Au. The nominal misfit δ between the two phases and the residual misfit $\Delta\epsilon$ between two crystalline supercells can be defined as[15]

$$\delta = \frac{2(a_{\mathrm{Cu}} - a_{\mathrm{Au}})}{a_{\mathrm{Cu}} + a_{\mathrm{Au}}}, \Delta\epsilon = \frac{2(na_{\mathrm{Cu}} - ma_{\mathrm{Au}})}{na_{\mathrm{Cu}} + ma_{\mathrm{Au}}}, \tag{1}$$

where n and m are the numbers of unit cells of the Cu and Au supercells that constitute the individual layers in the bicrystal stack. We used $m_{\mathrm{Au}} = 24$ and $n_{\mathrm{Cu}} = 27$ resulting in a residual misfit of $\Delta\epsilon = 0.25\%$ while keeping the overall size small enough for our simulation methods. The total number of atoms in our simulation cell was $\sim 10^6$.

We employed a binary Cu-Au embedded atom method (EAM) potential to describe the interatomic interactions. The potential is based on two well-established unary EAMs for

Cu[16] and Au[17]. The cross-potential that describes the interaction between Cu and Au was fitted to properly describe the Cu_3Au, CuAu and $CuAu_3$ intermetallic phases. The details of this potential will be published elsewhere[18].

The intermixing process that occurs between the Cu and Au crystal involves processes at a timescale not readily accessible by molecular dynamics methods, such as interdiffusion of Cu and Au atoms at the interface during the deposition process. In order to mimic this process, we intermixed the interface between Cu and Au layers manually by randomly flipping Cu and Au atoms over the interface to arrive at a specific concentration profile $c_w(z)$. The coordinate z here denotes the distance from the ideal interface and w is a measure for the initial width of the interface. The functional form of $c_w(z)$ was obtained by solving Fick's diffusion equations for interdiffusion in two semi-infinite bodies,

$$c_w(z) = \frac{1}{2} + \frac{1}{2}\mathrm{erf}\left(\frac{x}{w}\right). \tag{2}$$

The final atomic system with such a manually intermixed layer is shown in Fig. 1b.

After artificially intermixing the two crystals, we annealed the system at 1000 K for a total of 2 ns in molecular dynamics (MD) and then quenched it down to 300 K at a rate of 350 K/ns. This was followed by further ageing the system at 300 K for 1 ns. The resulting atomic configuration is shown in Fig. 1c. During these MD simulations, the temperature was controlled using a Langevin thermostat with a relaxation time of 1 ps. We used an anisotropic Berendsen barostat[19] with a relaxation time of ~ 5 ps to maintain zero stress along the $[112]$ and $[110]$ directions. All calculation steps were performed with a timestep of 5 fs.

As a final step in our analysis, we used the adaptive common neighbours analysis (CNA)[20,21] to identify and isolate defects in the crystal. The result of this analysis is exemplarily shown in Fig. 1d, where all atoms except for those being in an ideal face-centred cubic (FCC) structure are shown. This analysis allows us to characterise the resulting interface with respect to the defects formed at or near it.

3 Results

Fig. 2a shows the fraction of atoms that are not FCC in slices of constant thickness parallel to the $(\bar{1}\bar{1}1)$ plane. We will refer to this quantity as the defect concentration in what follows. While there are slight fluctuations with position, the defect concentration appears rather homogeneous throughout the volume even though the initial atomic concentration had a gradient. Clearly, the width of the interface grows with increasing intermixing width w.

Fig. 2b shows the interface width as a function of the initial intermixing width w. The interface width is defined as the distance between topmost and bottommost hexagonal close packed (HCP) atom perpendicular to the interface plane. The figure shows that the defect zone grows monotonously with increasing intermixing parameter w. For $w < 4$ nm the interface width is roughly $w/2$, while for $w > 4$ nm a larger fraction of the intermixed region develops stacking faults. The maximum width of the defected region along the $[\bar{1}\bar{1}1]$ axis is about 7 nm when the intermixing width of the two crystals is $w = 10$ nm, the maximum value investigated here.

Fig. 3 shows a series of views onto the interfacial plane. Shown are defects, i.e. all atoms except for those locally in an FCC neighbourhood, in the interfacial atomic region

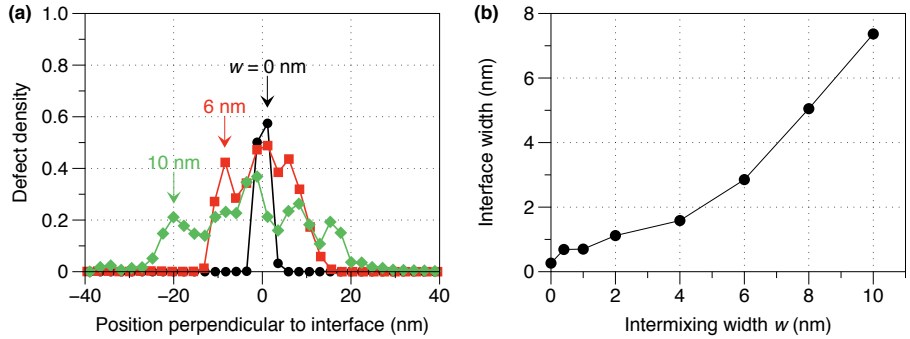

Figure 2. (a) Defect density, the fraction of atoms not in an FCC environment in slices parallel to the heterointerface, as a function of distance from the initial interface. (b) Interface width, measured as the distance between top- and bottommost HCP atom perpendicular to the heterointerface, as a function of the width of the initial intermixed layer w.

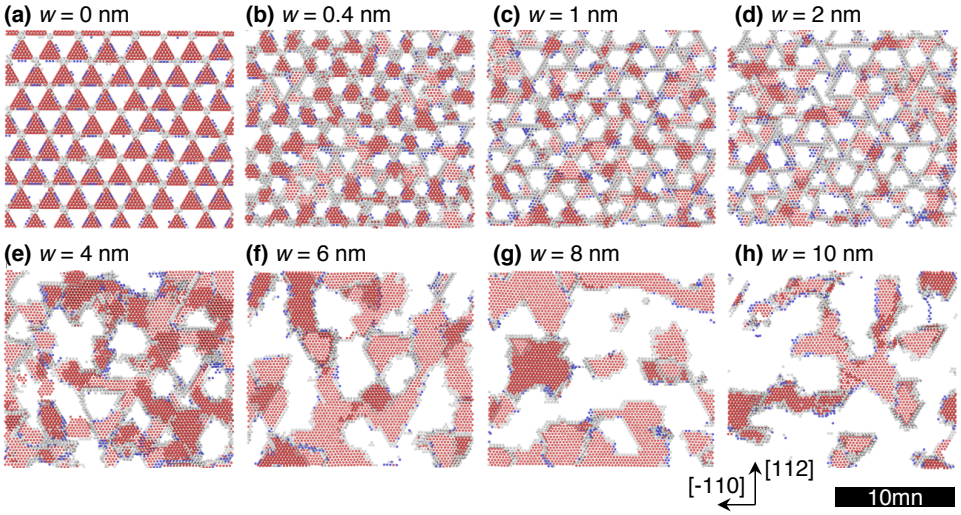

Figure 3. Atoms not in an FCC environment within a central slice of 1 nm thickness for intermixing width w of (a) 0 nm, (b) 0.4 nm, (c) 1 nm, (d) 2 nm, (e) 4 nm, (f) 6 nm, (g) 8 nm and (h) 10 nm. Atoms are colour coded according to their local lattice structure with HCP atoms in red, BCC atoms in blue and structures not identified in the common neighbour analysis in white.

± 0.5 nm around the initial interface. The sequence of panels (a) to (h) represents the structure of the interface for intermixing parameters from $w = 0$ nm to $w = 10$ nm. Fig. 3a ($w = 0$ nm) shows a perfect triangular network of HCP atoms. These are stacking faults that are bounded by Shockley partial dislocations. This network becomes distorted at $w = 0.4$ nm (Fig. 3b). The interfacial stacking faults are at this point no longer located exactly at the initial Cu|Au interface but start spreading into the material away from the interfacial plane. The regular structure of the network becomes even more distorted for

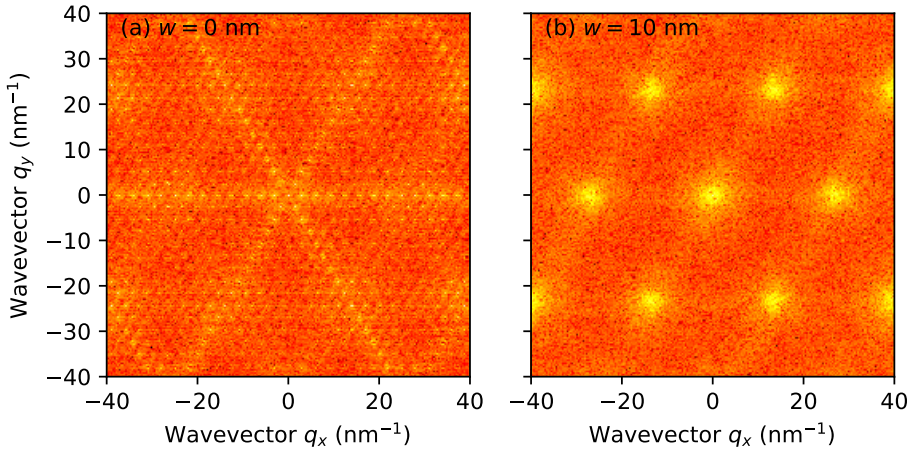

Figure 4. Two-dimensional structure factor of HCP atoms in a 0.5 nm slice around the heterointerface for (a) intermixing width $w = 0$ nm and (b) $w = 10$ nm.

$w = 1$ nm and 2 nm (Figs. 3c and d). At $w = 4$ nm (Fig. 3e) the regular pattern is no longer visible. The stacking faults follow a seemingly random pattern. At larger intermixing parameters, $w = 6$ nm, 8 nm and 10 nm (Figs. 3f, g and h) the interface is covered by large continuous patches of stacking faults with geometries reminiscent of slit islands[22]. A side view of the defects at $w = 10$ nm, the largest intermixing width, is shown in Fig. 1d. Fig. 1d directly illustrates that stacking faults do form not only on the $(\bar{1}\bar{1}1)$ plane perpendicular to the heterointerface but spread into the bulk of the material on the three other $\{111\}$ planes. The triangular stacking fault indicated by an arrow in this figure is one side of a stacking fault tetrahedron.

We now characterise the interface structure using two statistical measures. First, we compute the two-dimensional structure factor of all HCP atoms in a region ± 0.25 nm around the initial interface. The structure factor is given by

$$S(q_x, q_y) \propto \sum_{i,j} f_i f_j e^{i\vec{q}\cdot(\vec{r}_i - \vec{r}_j)} \tag{3}$$

where $\vec{q} = (q_x, q_y, 0)$ is the wavevector inside the interface plane, $\vec{r}_i$ is the position of atom i and the sum runs over all atoms in the system. The form factor f_i is unity for HCP atoms and zero otherwise. The two-dimensional map of $S(q_x, q_y)$ is shown in Fig. 4 for $w = 0$ nm (panel a) and $w = 10$ nm (panel b). Both figures show the underlying symmetry of the (111) plane with respective peaks at $2\pi/a_0$, where a_0 is the lattice constant. The ideal interface (Fig. 4a) shows individual peaks with a spacing of $\Delta q \sim 3$ nm^{-1} corresponding to ~ 2 nm wavelength. This structure is no longer visible for the disordered interface with $w = 10$ nm (Fig. 4b).

The conjugate measure to the structure factor is the radial distribution function (RDF),

$$g_2(r) \propto \sum_{ij} f_i f_j \delta\left(r - \sqrt{(x_i - x_j)^2 + (y_i - y_j)^2}\right), \tag{4}$$

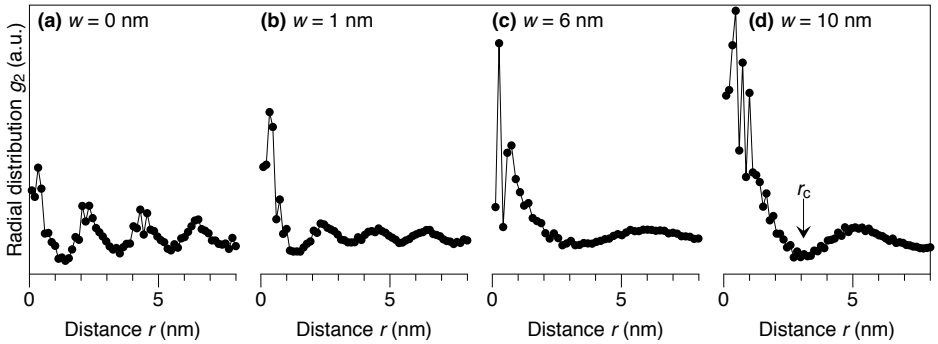

Figure 5. Two-dimensional radial distribution function of HCP atoms in a 0.5 nm slice around the heterointerface for intermixing with of (a) $w = 0$ nm, (b) 1 nm, (c) 6 nm and (d) 10 nm.

where x_i and y_i are the x- and y-positions of atom i, respectively. The xy-plane is the plane of the heterointerface. Fig. 5 shows the RDF for four interface widths. The sharp interface (Fig. 5a) shows pronounced oscillations with a first minimum at ~ 1.5 nm. As the interface width increases, the period of oscillation increases and for $w = 10$ nm, the first minimum has moved to ~ 3 nm.

4 Discussion

The perfectly sharp Cu|Au interface shown in Fig. 3a is a realisation of a semi-coherent interface, such as those found between immiscible compounds such as Cu|Ni[14]. The structure factor (Fig. 4a) and RDF (Fig. 5a) both show the periodicity of the triangular lattice of stacking faults. The first minimum in the RDF characterises the typical spacing between the triangles.

The semi-coherent character of the interface is lost as it becomes more disordered by intermixing. The primary defect at the interface is still the stacking fault, but the fault is no longer located at exactly the midplane between the two phases. The triangular structure of the stacking fault lattice is also lost at larger intermixing width. Fig. 1d illustrates that the majority of these faults are located on the interfacial $(\bar{1}\bar{1}1)$ plane, but that at larger width w the interfaces have a tendency to form stacking fault tetrahedra. Since these tetrahedra are sessile, they are often responsible for hardening, embrittlement or plastic instabilities[23].

The spacing of faulted and ideal crystalline regions can be estimated from the RDFs presented in Fig. 5. The minimum of the RDF corresponds to the distance from an HCP atom where the likelihood of finding another HCP atom is minimal. For the semi-coherent interface (Fig. 5a), this corresponds to the size of spacing between the triangular faults. For the disordered interfaces, this gives an approximate measure of the spacing between faulted regions. At $w = 10$ nm, the distance (indicated by an arrow in Fig. 5d) is around 3 nm, about half the total interface width of 7 nm (see Fig. 2b) and about double the spacing of ~ 1.5 nm between the triangles of the sharp interface ($w = 0$ nm).

5 Summary & Conclusions

We have shown that as a diffusive intermixed region develops at the heterointerface in the miscible Cu|Au system, the interface develops from an ordered two-dimensional network of triangular stacking faults to a three-dimensional network spreading in both crystals. This transformation increases the spacing of dislocations at the interface and gives rise to dislocation self-organisation into stacking fault tetrahedra. These changes in interface structure will have an influence on dislocations interacting with the interface and therefore the mechanical property of Cu|Au nanolaminates.

Acknowledgements

We used LAMMPS[24] for molecular dynamics calculations and OVITO[21] for visualisation and post processing of the molecular dynamics trajectories. This work was partially funded by a Helmholtz/Chinese Academy of Sciences Joint Research Group and the Deutsche Forschungsgemeinschaft (grant PA 2023/2). The authors gratefully acknowledge the Gauss Centre for Supercomputing e.V. (`www.gauss-centre.eu`) for funding this project by providing computing time through the John von Neumann Institute for Computing (NIC) on the GCS Supercomputer JUQUEEN at Jülich Supercomputing Centre (JSC).

References

1. G. S. Was and T. Foecke, *Deformation and fracture in microlaminates*, Thin Solid Films, **286**, 1–31, 1996.
2. A. Misra, M. Verdier, Y. C. Lu, H. Kung, T. E. Mitchell, M. Nastasi, and J. D. Embury, *Structure and mechanical properties of Cu-X (X = Nb,Cr,Ni) nanolayered composites*, Scr. Mater., **39**, 555–560, 1998.
3. B. M. Clemens, H. Kung, and S. A. Barnett, *Structure and Strength of Multilayers*, MRS Bull., **24**, 20–26, 1999.
4. P. M. Anderson, T. Foecke, and P. M. Hazzledine, *Dislocation-Based Deformation Mechanisms in Metallic Nanolaminates*, MRS Bull., **24**, 27–33, 1999.
5. A. Misra and H. Krug, *Deformation Behavior of Nanostructured Metallic Multilayers*, Adv. Eng. Mater., **3**, 217–222, 2001.
6. J. Wang and A. Misra, *An overview of interface-dominated deformation mechanisms in metallic multilayers*, Curr. Opin. Solid State Mater. Sci., **15**, 20–28, 2011.
7. J. Wang, R. G. Hoagland, J. P. Hirth, and A. Misra, *Atomistic simulations of the shear strength and sliding mechanisms of copper–niobium interfaces*, Acta Mater., **56**, 3109–3119, 2008.
8. F. Delogu and G. Cocco, *Molecular dynamics investigation on the role of sliding interfaces and friction in the formation of amorphous phases*, Phys. Rev. B., **71**, 144108, 2005.
9. G. Kaupp, *Mechanochemistry: the varied applications of mechanical bond-breaking*, CrystEngComm, **11**, 388–403, 2009.
10. J. A. Borders, *Ion back-scattering analysis of interdiffusion in Cu-Au thin films*, Thin Solid Films, **19**, 359–370, 1973.

11. W. M. Paulson and J. E. Hilliard, *Interdiffusion in compositionmodulated coppergold thin films*, J. Appl. Phys., **48**, 2117–2123, 1977.
12. Y. P. Li, X. F. Zhu, G. P. Zhang, J. Tan, W. Wang, and B. Wu, *Investigation of deformation instability of Au/Cu multilayers by indentation*, Philos. Mag., **90**, 3049–3067, 2010.
13. D. Cheng, Z. Jun Yan, and L. Yan, *Misfit dislocation network in Cu/Ni multilayers and its behaviors during scratching*, Thin Solid Films, **515**, 3698–3703, 2007.
14. S. Shao, J. Wang, A. Misra, and R. G. Hoagland, *Spiral Patterns of Dislocations at Nodes in (111) Semi-coherent FCC Interfaces*, Sci. Rep., **3**, 2448, 2013.
15. P. Gumbsch, *Atomistic study of misfit accommodation in cube-on-cube oriented Ag/Ni heterophase boundaries*, Z. Metallkd., **83**, 500–507, 1992.
16. Y. Mishin, M. J. Mehl, D. A. Papaconstantopoulos, A. F. Voter, and J. D. Kress, *Structural stability and lattice defects in copper: Ab initio, tight-binding, and embedded-atom calculations*, Phys. Rev. B, **63**, 224106, 2001.
17. G. Grochola, S. P. Russo, and I. K. Snook, *On fitting a gold embedded atom method potential using the force matching method*, J. Chem. Phys., **123**, 204719, 2005.
18. A. Gola, L. Pastewka, in preparation.
19. H. J. C. Berendsen, J. P. M. Postma, W. F. van Gunsteren, A. DiNola, and J. R. Haak, *Molecular dynamics with coupling to an external bath*, J. Chem. Phys., **81**, 3684–3690, 1984.
20. J. D. Honeycutt and H. C. Andersen, *Molecular dynamics study of melting and freezing of small Lennard-Jones clusters*, J. Phys. Chem., **91**, 4950–4963, 1987.
21. A. Stukowski, *Visualization and analysis of atomistic simulation data with OVITO–the Open Visualization Tool*, Model. Simul. Mater. Sci. Eng., **18**, 015012, 2010.
22. B. B. Mandelbrot, *The Fractal Geometry of Nature*, W. H. Freeman, 1982.
23. E. Martínez and B. P. Uberuaga, *Mobility and coalescence of stacking fault tetrahedra in Cu*, Sci. Rep., **5**, 9084, 2015.
24. S. Plimpton, *Fast parallel algorithms for short-range molecular dynamics*, J. Comput. Phys., **117**, 1–19, 1995.